

Composing Limit Cycles for Motion Planning of 3D Bipedal Walkers

Mohamad Shafiee Motahar, Sushant Veer, and Ioannis Poulakakis

Abstract—This paper presents a framework for navigation of 3D dynamically walking bipeds. The framework is based on extracting gait primitives in the form of limit-cycle locomotion behaviors, which are then composed by a higher-level planning algorithm with the purpose of navigating the biped to a goal location while avoiding obstacles. By formulating motion planning as a discrete-time switched system with multiple equilibria—each corresponding to a gait primitive—we provide analytical conditions that constrain the frequency of the switching signal so that the biped is guaranteed to stably execute a suggested plan. Effectively, these conditions distill the stability limitations of the system dynamics in a form that can be readily incorporated to the planning algorithm. We demonstrate the feasibility of the method in the context of a 3D bipedal model, walking dynamically under the influence of a Hybrid Zero Dynamics (HZD) controller. It is shown that the dimensional reduction afforded by HZD greatly facilitates the application of the method by allowing certificates of stability for gait primitives using sums-of-squares programming.

I. INTRODUCTION

Navigation of dynamically walking¹ bipeds amidst obstacles entails two hierarchically organized components. At the high level, a planner generates an obstacle-free path that conforms to the geometry of the environment. At the low level, a locomotion controller must execute the descending plan, while ensuring stable operation of the platform. When the high-level planning and low-level stability objectives are treated in isolation, the platform may not be able to faithfully execute the plan, or may fail due to instability. This paper proposes a framework that integrates locomotion control with motion planning to enable a 3D dynamically walking biped navigate in an environment cluttered by obstacles.

Motion planning for legged systems has been studied extensively in the context of humanoid robots walking under the Zero Moment Point (ZMP) stability criterion. Owing to the analytical nature of the ZMP, efficient planning algorithms have been employed to compute motion plans that comply with low-level ZMP stability requirements and achieve desired high-level objectives in high-dimensional spaces. The recent book [1] provides an extensive account of various approaches for motion planning in the context of humanoid robots, including footstep and whole-body planning, and motion planning with manipulation constraints. Based on novel formulations of such tasks as optimization problems, [2] provides an integrated approach to locomotion

planning, estimation and control for humanoid robots, which has been experimentally verified on the humanoid Atlas.

In stark contrast to ZMP-based humanoid robots, locomotion control methods for dynamically walking bipeds have been developed largely *in isolation* from high-level motion planning objectives. Indeed, most of the existing literature on dynamic walkers focuses on designing low-level controllers for generating and stabilizing periodic motions either for planar [3]–[5] or 3D [6]–[9] bipeds, for incorporating interaction forces [10]–[12], and for establishing robustness [13]–[15].

There are only very few works that explicitly take into account high-level motion planning objectives—e.g., avoid unsafe regions on the terrain or in the robot’s workspace—for limit-cycle walkers. In the context of footstep planning, [16] uses an energy-based planner to construct suitable sequences of limit cycles to realize walking over known uneven terrain for an underactuated planar biped. Emphasizing guaranteed performance, [17] proposed a method for safety-critical footstep planning by combining state-based constraints through quadratic programming with control Lyapunov functions [5]. Beyond planar bipeds—to the best of the authors’ knowledge—only [18] considers the problem of navigating a 3D limit-cycle walker to a desired goal location while avoiding obstacles. In [18], motion planning is formulated as a switched system with multiple equilibria, each corresponding to a limit-cycle walking behavior. The existence of a lower bound on the dwell time of the switching signal is established—but its value is estimated *numerically* using exhaustive simulations—so that stable composition of motion primitives can be achieved.

In this paper, we treat motion planning as a switched system, and we offer an *analytical* expression for the lower bound on the dwell time that guarantees stable execution of the suggested plan. Furthermore, we prove that the evolution of the state of the switching system is confined within a compact set, which can be explicitly characterized as the union of sub-level sets of Lyapunov functions, each corresponding to a gait primitive. The approach is implemented on an underactuated 3D biped, and locally exponentially stable gait primitives are extracted using Hybrid Zero Dynamics (HZD) controllers. The dimensional reduction afforded by HZD allows the estimation of the basin of attraction of the gait primitives using sums-of-squares (SOS) techniques, which facilitates the computation of the bound on the dwell time. It is worth noting that the proposed approach does not depend on the method used to design the underlying limit-cycle motion primitives. Moreover, it can be used to plan motions in other systems, which—like dynamically walking bipeds—move through their environment via cyclic interactions.

M. S. Motahar, S. Veer and I. Poulakakis are with the Department of Mechanical Engineering, University of Delaware, Newark, DE 19716, USA; e-mail: {motahar, veer, poulakas}@udel.edu.

This work is supported in part by NSF CAREER Award IIS-1350721 and NSF grant NRI-1327614.

¹Here the term “dynamically walking” indicates limit-cycle walkers.

II. A MODEL OF 3-D BIPEDAL WALKING

We consider a fairly generic model of a three-dimensional (3-D) bipedal walker as shown in Fig. 1. The model is composed of a torso and two identical legs, each connected to the torso via a two degree-of-freedom (DOF) revolute hip joint. The legs are composed of two links, the thigh and the shin, which are connected through a one DOF revolute knee joint. We assume that the stance foot acts as a pivot with three rotational DOFs corresponding to the yaw q_1 , pitch q_2 , and roll q_3 angles; see Fig. 1. In total, during the single support phase, the model has nine degrees of freedom $q := (q_1, \dots, q_9)^T \in \mathcal{Q}$, where \mathcal{Q} contains physically reasonable configurations of the system. Seven actuators—four located at the hip joints, two at the knee joints and one at the roll joint of the foot—provide the input torques.

Due to the nontrivial length of the hip joint, the equations of motion during the left and right leg support phases are different. In what follows, we develop a model for the left leg support phase; the equations for the right leg can be derived in a similar manner. The dynamics of the biped in the swing phase can be written as

$$D(q)\ddot{q} + C(q, \dot{q})\dot{q} + G(q) = Bu, \quad (1)$$

where $D(q)$ is the mass matrix, $C(q, \dot{q})\dot{q}$ contains the centrifugal and Coriolis forces and $G(q)$ contains the gravitational forces. The matrix B distributes the inputs u to the configuration variables q .

Defining $\hat{x} := (q^T, \dot{q}^T)^T$, the model can be written as

$$\dot{\hat{x}} = f(\hat{x}) + g(\hat{x})u, \quad (2)$$

where $\hat{x} \in T\mathcal{Q} := \{(q^T, \dot{q}^T)^T \mid q \in \mathcal{Q}, \dot{q} \in \mathbb{R}^9\}$ and the vector fields f and g are defined accordingly.

The continuous evolution of the swing dynamics (2) is interrupted when the swing leg hits the ground; i.e., when the state crosses the surface

$$\mathcal{S} := \{\hat{x} \in T\mathcal{Q} \mid p_{\text{foot}}^v(q) = 0, \dot{p}_{\text{foot}}^v(\hat{x}) < 0\}, \quad (3)$$

where p_{foot}^v denotes the vertical position of the foot of the swing leg. As in [8], the impact is assumed instantaneous and purely plastic, and can be modeled as a discrete map $\Delta : \mathcal{S} \rightarrow T\mathcal{Q}$, as

$$\hat{x}^+ = \Delta(\hat{x}^-). \quad (4)$$

The derivation of the map Δ also involves the transformation of coordinates from left leg support to right leg support; see [8] for more details.

III. GAIT PRIMITIVES

This section exploits the structure of the Poincaré map to extract a family of exponentially stable gait primitives, which are then concatenated by a planning algorithm to achieve desired objectives, such as reaching a goal position in the biped's workspace while avoiding obstacles on the way.

We begin by assuming the availability of a family of locally Lipschitz feedback control laws $\Gamma_p : T\mathcal{Q} \rightarrow \mathbb{R}^7$,

$$u = \Gamma_p(\hat{x}) \quad (5)$$

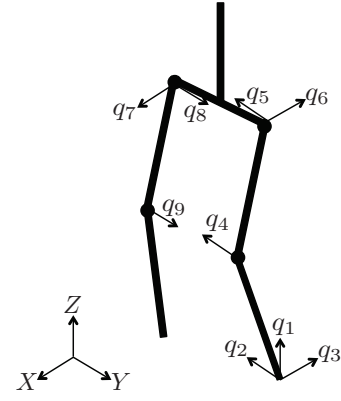


Fig. 1. Robot model with a choice of generalized coordinates when supported on left leg.

indexed by $p \in \mathcal{P}$, where \mathcal{P} is a finite index set corresponding to controllers that enable straight line and turning motions. Such controllers can be designed using a variety of methods, including [6]–[9]; for concreteness, in Section V below we will use HZD to design Γ_p . The dynamics of the biped in closed loop with the control law (5) can be expressed in the form of a system with impulse effects,

$$\Sigma_p : \begin{cases} \dot{\hat{x}} = f_p(\hat{x}), & \hat{x} \notin \mathcal{S} \\ \hat{x}^+ = \Delta(\hat{x}^-), & \hat{x}^- \in \mathcal{S} \end{cases}, \quad (6)$$

where $f_p(\hat{x}) := f(\hat{x}) + g(\hat{x})\Gamma_p(\hat{x})$, for $p \in \mathcal{P}$.

Let $\varphi_p(t, \hat{x}_0)$ be the maximal solution based on the initial condition $\hat{x}_0 \in T\mathcal{Q}$ of the continuous-time part of the closed loop system Σ_p defined by (6). The time-to-impact function $\hat{T}_{I,p} : T\mathcal{Q} \rightarrow \mathbb{R}_+$ can then be defined as

$$\hat{T}_{I,p}(\hat{x}) = \inf\{t \geq 0 \mid p_{\text{foot}}^v \circ \varphi_p(t, \Delta(\hat{x})) = 0\}. \quad (7)$$

Note that, for each $p \in \mathcal{P}$, the time-to-impact function (7) is independent of the yaw angle, q_1 , since the height of the swing foot p_{foot}^v does not depend on q_1 .

To study periodic solutions of Σ_p , $p \in \mathcal{P}$, we define the Poincaré return map $\hat{P}_p : \mathcal{S} \rightarrow \mathcal{S}$ as

$$\hat{P}_p(\hat{x}) := \varphi_p(\hat{T}_{I,p}(\hat{x}), \Delta(\hat{x})), \quad (8)$$

that transfers the state $\hat{x}[k]$ one step ahead; i.e.

$$\hat{x}[k+1] = \hat{P}_p(\hat{x}[k]). \quad (9)$$

The following Proposition is based on observations in [8], and it shows that restricting the choice of feedback controllers (5) so that they do not depend on the yaw angle q_1 results in a symmetry property of the Poincaré map.

Proposition 1: Let q_1 denote the yaw angle and $x := (\hat{x}_2, \dots, \hat{x}_{18})^T$ and define the group action

$$\Psi_g(\hat{x}) = (q_1 + g, x^T)^T. \quad (10)$$

Then, if the control law (5) is independent of the yaw angle q_1 , the corresponding Poincaré map \hat{P}_p is equivariant under the action of Ψ_g , i.e.

$$\hat{P}_p \circ \Psi_g(\hat{x}) = \Psi_g \circ \hat{P}_p(\hat{x}). \quad (11)$$

As a result, the Poincaré map can be written as

$$\hat{P}_p(\hat{x}) = \begin{bmatrix} q_1 + P_p^{(q_1)}(x) \\ P_p(x) \end{bmatrix}, \quad (12)$$

where $q_1 + P_p^{(q_1)}$ and P_p are the projections of \hat{P}_p onto q_1 and x , respectively.

Proof: Equation (11) is proved in [8, Proposition 3]. For (12), note that for any $\hat{x} = [q_1, x^T]^T$, (10) and (11) imply

$$\begin{aligned} \hat{P}_p([q_1, x^T]^T) &= \hat{P}_p \circ \Psi_{q_1}([0, x^T]^T) = \Psi_{q_1} \circ \hat{P}_p([0, x^T]^T) \\ &= \begin{bmatrix} q_1 + \Pi_{q_1} \circ \hat{P}_p([0, x^T]^T) \\ \Pi_x \circ \hat{P}_p([0, x^T]^T) \end{bmatrix} \end{aligned}$$

for any arbitrary q_1 , where Π_{q_1} and Π_x project the state onto its q_1 and x components, respectively. Defining $P_p^{(q_1)}(x) := \Pi_{q_1} \circ \hat{P}_p([0, x^T]^T)$ and $P_p(x) := \Pi_x \circ \hat{P}_p([0, x^T]^T)$, which are independent of q_1 , completes the proof. ■

The structure of the Poincaré map established by Proposition 1 allows the extraction of gait primitives suitable for navigation purposes in workspaces cluttered by obstacles. Intuitively, these gait primitives correspond to cyclic locomotion patterns—that is, limit cycles—which result in a net change of the heading angle. In more detail, such motions can be computed by requiring the condition

$$x_p^* = P_p(x_p^*), \quad (13)$$

i.e., that x_p^* is a fixed point of P_p defined by the decomposition of the Poincaré map (12). A gait primitive can now be defined as a pair $\mathcal{G}_p = \{P_p, x_p^*\}$. If all the eigenvalues of the linearization $A_p := \left. \frac{\partial P_p(x)}{\partial x} \right|_{x=x_p^*}$ of P_p in (12) are located within the unit disc centered at the origin, the fixed point x_p^* is locally exponentially stable, and so is the corresponding gait primitive \mathcal{G}_p . The basin of attraction of the fixed point x_p^* is defined as

$$\text{BoA}(x_p^*) = \left\{ x \in \mathcal{S} \mid \lim_{k \rightarrow \infty} P_p^k(x) = x_p^* \right\}, \quad (14)$$

where P_p^k denotes the composition of P_p with itself k times when it is defined. In Section V-C.1 below, we characterize the basin of attraction associated with a fixed point x_p^* using sums-of-squares programming. Finally, note that associated with a gait primitive \mathcal{G}_p is a change in the heading angle s , which can be computed by

$$s = P_p^{(q_1)}(x_p^*). \quad (15)$$

IV. STABLE SWITCHING AMONG MULTIPLE EQUILIBRIA

In what follows, we consider a collection $\mathbb{G} = \{\mathcal{G}_p, p \in \mathcal{P}\}$ of locally exponentially stable gait primitives. Note that \mathbb{G} provides actions in the form of nominal walking arcs—as will be defined in Section V-B below—to a planning algorithm, which is tasked to output a suitable sequence of gait primitives that achieve a desired objective. In this context, the planner concatenates gait primitives in \mathbb{G} according to a switching signal $\sigma : \mathbb{Z}_+ \rightarrow \mathcal{P}$ that maps the stride number k to the corresponding gait primitive $p = \sigma(k)$ that should

be executed in the current stride. This process gives rise to a discrete-time switched system

$$x[k+1] = P_{\sigma(k)}(x[k]), \quad (16)$$

which captures the dynamics of switching among gait primitives in \mathbb{G} . It is well known that switching among systems that share a common exponentially stable equilibrium may cause instability, and conditions to avoid such behaviors have been established [19]. However, (16) differs from those switched systems in that the individual maps $\{P_p, p \in \mathcal{P}\}$ do *not* share a common equilibrium. Hence, one cannot expect that the solution of (16) will converge to one of the equilibrium points. The main result of this section is to provide conditions that guarantee that the system's solution will not escape from a compact set that includes the equilibrium points for any switching sequence the planner requires, as long as this sequence respects a bound on the dwell time.

We work in an open connected set $\mathcal{D} \subset \mathcal{S}$ over which P_p is well defined for all $p \in \mathcal{P}$. As above, let x_p^* be a fixed point of P_p , and assume that $x_p^* \in \mathcal{D}$ for all $p \in \mathcal{P}$; that is, \mathcal{D} contains all the fixed points. Let $\sigma : \mathbb{Z}_+ \rightarrow \mathcal{P}$ be a switching signal with $p = \sigma(k)$, and let $\{k_1, k_2, \dots\}$ be the corresponding switching times. The dwell time $N_d \geq 1$ is an integer representing the minimum number of steps between two successive switches in σ ; that is, $\sigma(k_i + k) = \sigma(k_i)$ for all $k < N_d$.

Definition 1: A continuous function $V_p : \mathcal{D} \rightarrow \mathbb{R}$ is an exponential Lyapunov function, if for $x \in \mathcal{D}$

$$\chi_{p,1}(\|x - x_p^*\|) \leq V_p(x) \leq \chi_{p,2}(\|x - x_p^*\|), \quad (17)$$

$$V_p(x[k+1]) \leq \epsilon V_p(x[k]), \quad (18)$$

where $\chi_{p,1}, \chi_{p,2}$ are class- \mathcal{K} functions and $0 < \epsilon < 1$.

Following the set constructions in [20], we introduce subsets of \mathcal{D} , which are essential in presenting the main result of this section. For each $p \in \mathcal{P}$, let

$$\mathcal{N}_p(\kappa) := \{x \in \mathcal{D} \mid V_p(x) \leq \kappa\}, \quad (19)$$

and let the union of these sets over all $p \in \mathcal{P}$ be

$$\mathcal{N}(\kappa) := \bigcup_{p \in \mathcal{P}} \mathcal{N}_p(\kappa), \quad (20)$$

which is not necessarily connected. Next, define

$$\omega_p(\kappa) := \max_{x \in \mathcal{N}(\kappa)} V_p(x), \quad (21)$$

and let $\omega_{\max}(\kappa)$ and $\omega_{\min}(\kappa)$ be the maximum and minimum of $\omega_p(\kappa)$ over the finite index set \mathcal{P} , respectively. Let

$$\mathcal{M}_p(\kappa) := \{x \in \mathcal{D} \mid V_p(x) \leq \omega_p(\kappa)\}. \quad (22)$$

We complete our constructions by defining

$$\overline{\mathcal{M}}(\kappa) := \bigcup_{p \in \mathcal{P}} \mathcal{M}_p(\kappa), \quad \underline{\mathcal{M}}(\kappa) := \bigcap_{p \in \mathcal{P}} \mathcal{M}_p(\kappa). \quad (23)$$

Note that

$$\mathcal{N}(\kappa) \subset \underline{\mathcal{M}}(\kappa), \quad (24)$$

and that the set $\overline{\mathcal{M}}(\kappa)$ is connected.

With these definitions, we are ready to state the main result of this section, which guarantees that a solution of (16) that starts in $\underline{\mathcal{M}}(\kappa)$ will stay in $\overline{\mathcal{M}}(\kappa)$ for all future time steps, provided that a bound on the dwell time of the switching signal σ is respected.

Theorem 1: Consider (16) and assume that for each $p = \sigma(k) \in \mathcal{P}$ there exists a function $V_p : \mathcal{D} \rightarrow \mathbb{R}$ that satisfies the conditions of Definition 1. Let $\mu(\kappa) > 1$ be such that

$$\frac{V_{p_i}(x)}{V_{p_j}(x)} \leq \mu(\kappa), \quad \forall p_i, p_j \in \mathcal{P}, \quad \forall x \in \mathcal{D} \setminus \mathcal{N}(\kappa). \quad (25)$$

Assume further that the dwell time $N_d \in \mathbb{Z}_+$ of the switching signal σ satisfies

$$N_d \geq \frac{\log\left(\mu(\kappa) \frac{\omega_{\max}(\kappa)}{\omega_{\min}(\kappa)}\right)}{\log(1/\epsilon)}. \quad (26)$$

Then, for every initial condition in the set $\underline{\mathcal{M}}(\kappa)$, the solution of (16) remains in $\overline{\mathcal{M}}(\kappa)$.

Proof: Consider an arbitrary switching signal $\sigma : \mathbb{Z}_+ \rightarrow \mathcal{P}$ with switching times $\{k_1, k_2, \dots\}$. Without loss of generality, assume that the system starts at $k = 0$ and let $x[0] \in \underline{\mathcal{M}}(\kappa)$. This implies that $x[0] \in \mathcal{M}_p(\kappa)$ for all $p \in \mathcal{P}$ so that $x[0] \in \mathcal{M}_{\sigma(0)}(\kappa)$. Thus,

$$V_{\sigma(0)}(x[0]) \leq \omega_{\sigma(0)}(\kappa), \quad (27)$$

and by (18), $V_{\sigma(0)}(x[k]) \leq \omega_{\sigma(0)}(\kappa)$ for all $0 \leq k \leq k_1$, implying that $x[k] \in \mathcal{M}_{\sigma(0)}(\kappa) \subset \overline{\mathcal{M}}(\kappa)$ for all $0 \leq k \leq k_1$.

Note that, at the switching time k_1 , the state $x[k_1] \in \overline{\mathcal{M}}(\kappa)$, and we distinguish the following cases:

Case I: $x[k_1] \in \underline{\mathcal{M}}(\kappa)$. Then, arguing as above we have that $V_{\sigma(k_1)}(x[k_1]) \leq \omega_{\sigma(k_1)}(\kappa)$, and thus $x[k] \in \mathcal{M}_{\sigma(k_1)}(\kappa) \subset \overline{\mathcal{M}}(\kappa)$ over the interval $k_1 \leq k \leq k_2$.

Case II: $x[k_1] \in \overline{\mathcal{M}}(\kappa) \setminus \underline{\mathcal{M}}(\kappa)$. In fact, we will show by contradiction that this case is not possible due to the condition (26) imposed on the dwell time. By (24), $\mathcal{N}(\kappa) \subset \underline{\mathcal{M}}(\kappa)$ and thus the fact that $x[k_1] \notin \underline{\mathcal{M}}(\kappa)$ implies that $x[k_1] \notin \mathcal{N}(\kappa)$. Then, (25) can be used to obtain $V_p(x[k_1]) \leq \mu V_{\sigma(0)}(x[k_1])$ for all $p \in \mathcal{P}$, which by (18) results in $V_p(x[k_1]) \leq \mu \epsilon^{k_1} V_{\sigma(0)}(x[0])$ for all $p \in \mathcal{P}$. Then, since $k_1 \geq N_d$ by the definition of the dwell time, we obtain

$$V_p(x[k_1]) \leq \mu \epsilon^{N_d} V_{\sigma(0)}(x[0]) \quad \forall p \in \mathcal{P}. \quad (28)$$

In view of (26), we have $\mu \epsilon^{N_d} \leq \omega_{\min}(\kappa)/\omega_{\max}(\kappa)$, and by using (27) and (28) we obtain

$$V_p(x[k_1]) \leq \frac{\omega_{\min}(\kappa)}{\omega_{\max}(\kappa)} \omega_{\sigma(0)}(\kappa) \leq \omega_{\min}(\kappa) \quad \forall p \in \mathcal{P}, \quad (29)$$

which implies that for any $p \in \mathcal{P}$ that is ‘‘switched in’’ at k_1 , $x[k_1] \in \mathcal{M}_p(\kappa)$. Thus, $x[k_1] \in \underline{\mathcal{M}}(\kappa)$, which contradicts the initial assumption that $x[k_1] \in \overline{\mathcal{M}}(\kappa) \setminus \underline{\mathcal{M}}(\kappa)$, essentially guaranteeing that Case II does not emerge.

Hence, for any $x[0] \in \underline{\mathcal{M}}(\kappa)$, we have shown that $x[k] \in \overline{\mathcal{M}}(\kappa)$ over the interval $0 \leq k \leq k_1$. Then, the constraint (26) on the dwell time ensures that $x[k_1] \in \underline{\mathcal{M}}(\kappa)$ so that $x[k] \in \overline{\mathcal{M}}(\kappa)$ over the interval $k_1 \leq k \leq k_2$. Propagating this construction to future time steps proves the result. ■

An immediate consequence of Theorem 1 is the following Corollary that will be useful for our planning purposes.

Corollary 1: Under the assumptions of Theorem 1, for every initial condition in the set $\mathcal{N}(\kappa)$, the solution of (16) will remain in $\overline{\mathcal{M}}(\kappa)$ for all future times.

Theorem 1 has some important implications for planning. First, it provides a constraint on the switching signal that essentially captures the limitations imposed by the dynamics of the system as it switches among different gait primitives. Second, the constraint (26) is provided in closed form, and can easily be incorporated in the planning algorithm so that descending commands from the high-level planner respect the dynamics of the low-level platform. Third, Theorem 1 guarantees that the evolution of the state of (16) remains within the set $\overline{\mathcal{M}}(\kappa)$ defined by (23), the size of which can be adjusted through the parameter κ . Reducing the size of $\overline{\mathcal{M}}(\kappa)$ ensures smaller deviations from the nominal plan, at the expense of a larger lower bound on the dwell-time (26), which in turn reduces the flexibility of the planner in providing a path that respects the geometry of the workspace.

V. HZD BASED 3-D BIPED EXAMPLE

This section explores some of the implications of Theorem 1 in the context of the bipedal model of Fig. 1 walking under the influence of an HZD control law. It should be emphasized that the dimensional reduction afforded by HZD, greatly facilitates the set constructions of Theorem 1 and the verification of the basins of attraction of the corresponding gait primitives via established SOS techniques.

A. Controller Design

The controller is developed within the HZD framework as in [21]; thus the exposition will be terse. To the continuous dynamics (2), associate the output functions

$$y = h(q) := q_a - h_d(\theta(q)), \quad (30)$$

where $q_a := (q_3, \dots, q_9)^T$ includes the controlled variables and h_d denotes the desired evolution as a function of the monotonic quantity $\theta(q) = -q_2 - q_4/2$, which corresponds to the angle of the line connecting the foot of the support leg with the corresponding hip joint. As in [21, Section IV-B], h_d is designed using Bezier polynomials.

As in [21, Section V-A], we augment the output (30) with correction polynomials h_c , i.e.,

$$\bar{y} = \bar{h}(q, y_i, \dot{y}_i) := q_a - h_d(\theta) - h_c(\theta, y_i, \dot{y}_i), \quad (31)$$

where y_i and \dot{y}_i are the values of the (uncorrected) output (30) at the beginning of the step. The coefficients of the correction polynomials h_c are chosen so that they smoothly reject the initial error with respect to the (uncorrected) output (30) by the middle of the step; see [21] for details.

To induce turning on a straight walking gait, we augment the output (31) with polynomials h_s , i.e.,

$$\tilde{y} = \tilde{h}_p(q, y_i, \dot{y}_i) := q_a - h_d(\theta) - h_c(\theta, y_i, \dot{y}_i) - h_s(\theta, \beta_p), \quad (32)$$

where β_p is the vector parameters determined in a way that does not interfere with the design of h_c that renders the zero

dynamics surface \mathcal{Z} associated with the original output (30) hybrid invariant; see [21, Section VII.A] for more details. Then, selecting the control inputs according to

$$u = \Gamma_p(x) := L_g L_f \tilde{h}_p(x)^{-1} \left[v(\tilde{y}, \dot{\tilde{y}}) - L_f^2 \tilde{h}_p(x) \right], \quad (33)$$

where v is an auxiliary controller that renders the surface

$$\tilde{\mathcal{Z}}_p := \{(q, \dot{q}) \in T\mathcal{Q} \mid \tilde{h}_p(q, y_i, \dot{y}_i) = 0, L_f \tilde{h}_p(q, \dot{q}, y_i, \dot{y}_i) = 0\}$$

attractive and hybrid invariant under the flow of the system Σ_p defined by (6); the controller v can be designed as in [3] or [5], for example. It is important to emphasize that the control law (33) does *not* depend on the yaw angle q_1 due to the fact that the output (32) is independent of q_1 and by [8, Proposition 1] the dynamics is invariant under yaw rotations. Then, by Proposition 1 the closed-loop Poincaré map is equivariant under yaw rotations.

The hybrid invariance of $\tilde{\mathcal{Z}}_p$ ensures that the restriction $\hat{\rho}_p := \hat{P}_p|_{\mathcal{S} \cap \tilde{\mathcal{Z}}_p}$ of the Poincaré map \hat{P}_p defined by (8) on the surface $\mathcal{S} \cap \tilde{\mathcal{Z}}_p$ is well defined, and that $\hat{z} = (q_1, \dot{q}_1, \dot{\theta})^T$ is a valid set of coordinates on $\mathcal{S} \cap \tilde{\mathcal{Z}}_p$. Furthermore, as a result of equivariance the restricted Poincaré map can be decomposed as

$$\begin{bmatrix} q_1[k+1] \\ z[k+1] \end{bmatrix} = \begin{bmatrix} q_1[k] + \rho_p^{(q_1)}(z[k]) \\ \rho_p(z[k]) \end{bmatrix} =: \hat{\rho}_p(\hat{z}[k]). \quad (34)$$

where $z = (\dot{q}_1, \dot{\theta})^T$. Before we turn our attention to computing gait primitives, the following remark is in order.

Remark 1: We will assume that switchings among primitives occur *only* at the beginning of a stride. This assumption is typical in motion planning scenarios [18], and, while it does not significantly restrict the flexibility of the planner, it allows us to take advantage of the dimensional reduction afforded by HZD in a way that greatly simplifies the planning problem. In this case, switching from one primitive to another excites the uncorrected outputs (30) only when the stride begins; i.e., y_i and \dot{y}_i are non-zero. The correction polynomials h_c in (32) account for this excitation, and, by construction, they ensure that after the middle of the stride, the surface $\tilde{\mathcal{Z}}_p$ coincides with the zero dynamics surface \mathcal{Z} associated with the original output (30). Hence, at the end of the stride, the state is on $\mathcal{S} \cap \tilde{\mathcal{Z}}_p = \mathcal{S} \cap \mathcal{Z}$, independent of the perturbation introduced by the switching. As a result, HZD greatly facilitates planning by ensuring that, despite switching, the discrete evolution of the system always occurs on $\mathcal{S} \cap \mathcal{Z}$, allowing the use of the restricted Poincaré map (34) for planning.

B. Generating Gait Primitives

A number of gait primitives corresponding to walking straight and turning motions can be produced using the controller described above; Fig. 2 shows nominal walking arcs for a family of such motions. Note that a turning primitive associated with a net change s in the heading angle is generated by seeking for the fixed point x_p^* and the parameters β_p that satisfy (13) and (15). Additional constraints related to actuator limitations, foot-ground interaction and

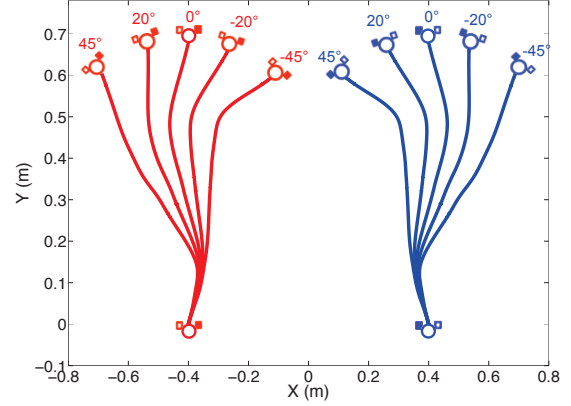


Fig. 2. Nominal walking arcs for family of gait primitives. The number on each arc shows the change in heading. Blue corresponds to turning when support is on the left leg and red when support is on the right leg.

other specifications can be incorporated in the computation of the fixed points as in [3, Section 3.2] and [21].

For the purpose of illustrating the method, we choose a gait basis set $\mathbb{G} = \{\mathcal{G}_0, \mathcal{G}_1, \mathcal{G}_2\}$, consisting of three gait primitives; namely, \mathcal{G}_0 for straight line motion, \mathcal{G}_1 for clockwise (CW) turning by 45° , and \mathcal{G}_2 for counterclockwise turning by 45° . The three gait primitives correspond to strides that begin with the left leg providing support. The sharp turning primitives in \mathbb{G} enable the biped to navigate through tight environments as will be shown in Section V-D. Each gait primitive produces a nominal walking arc—see Fig. 2 for examples of such arcs—which is characterized by a triplet (L_{cm}, s_{cm}, s) , where L_{cm} and s_{cm} denote the length and angle of the COM displacement vector, and s is the change in heading angle; for the gait primitives in \mathbb{G} , these quantities are given in Table I. A planning algorithm can concatenate these nominal walking arcs from a discrete set available to it to construct a path, as will be shown in Section V-D below.

TABLE I
SELECTED NOMINAL WALKING ARCS

Primitive	L_{cm} [m]	s_{cm} [deg]	s [deg]
Straight	0.6789	0	0
CW	0.6710	-25.05	-45
CCW	0.6558	26.21	45

C. Stable Composition of Gait Primitives

In this section we take advantage of the dimensional reduction afforded by the HZD method to estimate the basin of attraction of the gait primitives in \mathbb{G} using SOS techniques, and we use these results to facilitate the construction of the sets involved in Theorem 1, which is then applied to establish stable motion planning.

1) *Estimation of Basin of Attraction:* By Remark 1, the systems's nominal evolution is perturbed only at the beginning of a stride, thereby resulting in the reduced-order Poincaré map $\hat{\rho}_p$ defined by (34). Then, to estimate the basin

of attraction associated with a gait primitive, we will restrict our attention to the corresponding reduced-order system

$$z[k+1] = \rho_p(z[k]) , \quad (35)$$

which is two dimensional. Below we describe the process for one such system; i.e., for a fixed p . For simplicity, the corresponding fixed point is translated to the origin.

We begin by numerically estimating the domain of definition of ρ_p . This is achieved by radially propagating a closed disc around the origin and checking whether ρ_p is defined on sampled points on its boundary. We densely repeat this process until we obtain the maximum radius r_p that corresponds to the ball $\mathcal{B}_{r_p}(0)$ over which ρ_p is well defined.

Next, we turn our attention to estimating the basin of attraction of the equilibrium point of (35). Our estimate will have the form of a sub-level set $\{z \in \mathcal{B}_{r_p}(0) \mid V_p(z) \leq \eta\}$ of a quadratic Lyapunov function $V_p(z) := z^T S_p z$, where S_p is a positive definite matrix that solves the discrete Lyapunov equation of the linearization associated with (35). To check (18), we formulate a SOS feasibility program as in [22]

$$\begin{aligned} & \max \eta \\ & \text{s.t. } \eta < \lambda_{\min}(S_p) r_p^2 \\ & \quad b_p(z) \text{ is SOS} \\ & \epsilon V_p(z[k]) - V_p(z[k+1]) - b_p(z[k])(\eta - V_p(z[k])) \text{ is SOS} \end{aligned}$$

where r_p is the radius of the estimate of the domain of definition, $\lambda_{\min}(S_p)$ is the minimum eigenvalue of S_p , and $b_p(z)$ is a positive definite polynomial of z ; see [22]. The first condition ensures that the resulting estimate of the basin of attraction is entirely contained in the domain of definition. Note that ϵ is the rate of convergence, which according to the constructions of Theorem 1 will be the same for each system p . Finally, as in [22, Section 3.1.1] we approximate ρ_p in the neighborhood of the fixed point using Taylor series up to second-order terms to obtain a polynomial system as the SOS algorithm requires.

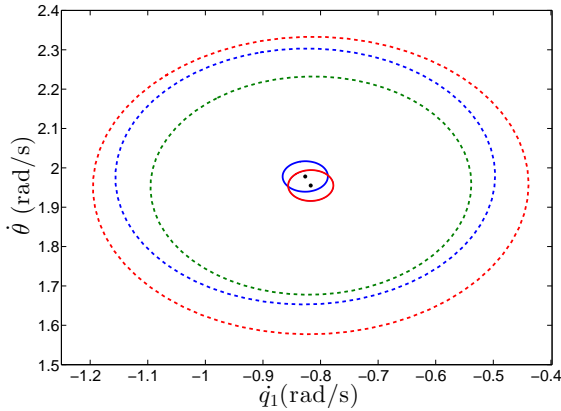


Fig. 3. Estimates of the basin of attraction for each of the gait primitives in \mathbb{G} (dashed ellipses), and computation of $\overline{\mathcal{M}}(\kappa)$ (union of solid ellipses), which is entirely inside the intersection of the basin of attractions. The colors blue, red and green correspond to the primitives \mathcal{G}_0 , \mathcal{G}_1 and \mathcal{G}_2 respectively. Note that the fixed points of \mathcal{G}_1 and \mathcal{G}_2 and their corresponding $\mathcal{M}(\kappa)$ sets are almost coinciding. The set $\overline{\mathcal{M}}(\kappa)$ of (23) corresponds to $\kappa = 0.0002$ resulting in the dwell time $N_d = 1$.

A sequence of SOS feasibility programs is then executed to obtain η_{\max} , beyond which the process fails to give a feasible solution. The procedure is carried out individually for all three motion primitives in \mathbb{G} , and the outcome is $\eta_0 = 0.11$, $\eta_1 = 0.15$ and $\eta_2 = 0.08$ corresponding to \mathcal{G}_0 , \mathcal{G}_1 , \mathcal{G}_2 , respectively. The resulting estimates of the basins of attraction are shown as dashed ellipses in Fig. 3. Clearly, all the fixed points lie in the intersection of basins of attraction.

2) Computation of Minimum Dwell Time for Stability:

Here we apply Theorem 1 to ensure that the switching frequency among the gait primitives guarantees that the evolution of the switched system remains within the desired safe region $\overline{\mathcal{M}}(\kappa)$. By the SOS program, it has been verified that the quadratic functions $V_p(z) := z^T S_p z$ satisfy the conditions in Definition 1 for all the gait primitives p with the same value of $\epsilon = 0.12$. To provide the planner with enhanced flexibility, it is desirable to have the ability to switch at every stride, implying that the desired value of the lower bound on the dwell time is $N_d = 1$. To determine if this dwell time is feasible, we must verify that, given $\epsilon = 0.12$ from the SOS program of Section V-C.1, there exists a κ for which the conditions of Theorem 1 are satisfied. This can be done by numerically computing $\omega_{\max}(\kappa)$, $\omega_{\min}(\kappa)$ using (21), and $\mu(\kappa)$ using (25) for a given κ . Then, we verify that (26) is satisfied by $N_d = 1$, implying that if the system starts in the set $\mathcal{N}(\kappa)$ defined by (20), its solution never escapes from $\overline{\mathcal{M}}(\kappa)$, which corresponds to the union of the solid ellipses in Fig. 3. In the example shown in Fig. 3, $\kappa = 0.0002$.

D. Path Planning

For the purpose of illustration, we consider the environments of Fig. 4, in which the bipedal model of Fig. 1 starts at an initial position and is required to reach the designated goal while avoiding obstacles in between. To obtain an obstacle-free path, we implement a Rapidly-exploring Random Tree (RRT) [23]. Based on the discussion above, the planner is allowed to switch primitives at every stride. With this a priori knowledge, the RRT planner constructs a nominal path, shown by the red circles in Fig. 4. It can be seen that in both environments the biped is able to closely follow the path and approach the goal without hitting the obstacles.

The environment shown in Fig. 4(a) is relatively tight given the dimensions of the biped. However, due to the enhanced flexibility offered to the planner by the sharp turning primitives and by the ability to switch at every stride, the biped reaches the goal in 24 strides with a small drifting error, approximately equal to 6.3cm. In the environment shown in Fig. 4(b), the biped takes 90 strides to reach the goal, and the final error is larger, approximately equal to 1.20m. Yet, this represents a considerable improvement with respect to [18], in which the biped drifts 2.59m away from the goal by the end of the plan. Most important, the analytically tractable procedure offered by Theorem 1 and the dimensional reduction afforded by HZD couple the relevant parameters ϵ and κ in an explicit way, which can be used to quantify the interplay between the geometry of the

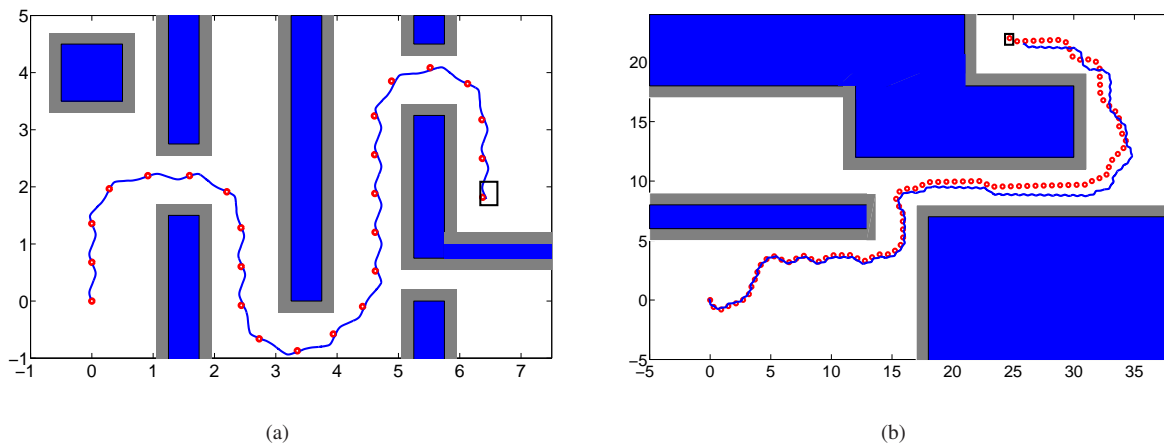


Fig. 4. Two walking environments. The nominal planned strides are shown as red circles and the simulated biped steps are indicated by blue lines. In the environment (a), the biped takes 24 strides to reach the goal (marked by black rectangle) and the final drifting error is 6.3 cm. In the environment (b), the biped takes 90 strides to reach the goal and the final error is 1.20 m.

environment and the error in the execution of a plan. This is the subject of ongoing work.

VI. CONCLUSION

This paper presents a framework for navigation of a 3D dynamically walking biped that offers analytically tractable stability guarantees. Gait primitives in the form of limit cycles are composed by a planning algorithm in a way that ensures stable operation under constrained switching that respects the biped's dynamics. The constraint is expressed analytically in the form of a bound on the dwell time of the switching signal. We demonstrate the method on a biped walking in closed loop with a HZD controller, and highlight the advantages of the dimensional reduction provided by HZD in establishing certificates of stability of the motion primitives using SOS programming. This work presents a step toward bridging the gap between high-level motion planning algorithms and low-level locomotion controllers in the context of dynamically walking bipeds.

REFERENCES

- [1] K. Harada, E. Yoshida, and K. Yokoi, Eds., *Motion Planning for Humanoid Robots*. Springer-Verlag, 2010.
- [2] S. Kuindersma, R. Deits, M. Fallon, A. Valenzuela, H. Dai, F. Permenter, T. Koolen, P. Marion, and R. Tedrake, "Optimization-based locomotion planning, estimation, and control design for the atlas humanoid robot," *Autonomous Robots*, vol. 40, pp. 429–455, 2016.
- [3] E. R. Westervelt, J. W. Grizzle, C. Chevallereau, J. H. Choi, and B. Morris, *Feedback Control of Dynamic Bipedal Robot Locomotion*. CRC Press, 2007.
- [4] L. B. Freidovich, U. Mettin, A. S. Shiriaev, and M. W. Spong, "A passive 2-dof walker: Hunting for gaits using virtual holonomic constraints," *IEEE Transactions on Robotics*, vol. 25, no. 5, pp. 1202–1208, 2009.
- [5] A. Ames, K. Galloway, J. Grizzle, and K. Sreenath, "Rapidly exponentially stabilizing control lyapunov functions and hybrid zero dynamics," *IEEE Transactions on Automatic Control*, vol. 59, no. 4, pp. 876–891, 2014.
- [6] R. D. Gregg and M. W. Spong, "Reduction-based control of three-dimensional bipedal walking robots," *The International Journal of Robotics Research*, vol. 29, no. 6, pp. 680–702, 2009.
- [7] R. W. Sinnet and A. D. Ames, "3D bipedal walking with knees and feet: A hybrid geometric approach," in *Proceedings of the IEEE Conference on Decision and Control*, 2009, pp. 3208–3213.
- [8] C.-L. Shih, J. Grizzle, and C. Chevallereau, "From stable walking to steering of a 3d bipedal robot with passive point feet," *Robotica*, vol. 30, no. 07, pp. 1119–1130, 2012.
- [9] K. A. Hamed and J. W. Grizzle, "Event-based stabilization of periodic orbits for underactuated 3-D bipedal robots with left-right symmetry," *IEEE Transactions on Robotics*, vol. 30, no. 2, pp. 365–381, 2014.
- [10] S. Veer, M. S. Motahar, and I. Poulakakis, "On the adaptation of dynamic walking to persistent external forcing using hybrid zero dynamics control," in *Proceedings of the IEEE/RSJ International Conference on Intelligent Robots and Systems*, 2015, pp. 997–1003.
- [11] M. S. Motahar, S. Veer, J. Huang, and I. Poulakakis, "Integrating dynamic walking and arm impedance control for cooperative transportation," in *Proceedings of the IEEE/RSJ International Conference on Intelligent Robots and Systems*, 2015, pp. 1004–1010.
- [12] S. Veer, M. S. Motahar, and I. Poulakakis, "Local input-to-state stability of dynamic walking under persistent external excitation using hybrid zero dynamics," in *Proceedings of the American Control Conference*, 2016, pp. 4801–4806.
- [13] C. O. Saglam and K. Byl, "Robust policies via meshing for metastable rough terrain walking," in *Proceedings of Robotics: Science and Systems*, vol. 7, 2014, pp. 129–143.
- [14] S. Kolathaya and A. D. Ames, "Parameter sensitivity and boundedness of robotic hybrid periodic orbits," *IFAC-PapersOnLine*, vol. 48, no. 27, pp. 377–382, 2015.
- [15] Q. Nguyen and K. Sreenath, "Optimal robust control for bipedal robots through control lyapunov function based quadratic programs," in *Proceedings of Robotics: Science and Systems*, 2015.
- [16] I. R. Manchester and J. Umenberger, "Real-time planning with primitives for dynamic walking over uneven terrain," in *Proceedings of the IEEE International Conference on Robotics and Automation*, 2014, pp. 4639–4646.
- [17] Q. Nguyen and K. Sreenath, "Safety-critical control for dynamical bipedal walking with precise footstep placement," *IFAC-PapersOnLine*, vol. 48, no. 27, pp. 147–154, 2015.
- [18] R. D. Gregg, A. K. Tilton, S. Candido, T. Bretl, and M. W. Spong, "Control and planning of 3-d dynamic walking with asymptotically stable gait primitives," *IEEE Transactions on Robotics*, vol. 28, no. 6, pp. 1415–1423, 2012.
- [19] D. Liberzon, *Switching in Systems and Control*. Birkhäuser, 2003.
- [20] T. Alpcan and T. Basar, "A stability result for switched systems with multiple equilibria," *Dynamics of Continuous, Discrete and Impulsive Systems Series A: Mathematical Analysis*, vol. 17, pp. 949–958, 2010.
- [21] C. Chevallereau, J. W. Grizzle, and C.-L. Shih, "Asymptotically stable walking of a five-link underactuated 3-d bipedal robot," *IEEE Transactions on Robotics*, vol. 25, no. 1, pp. 37–50, 2009.
- [22] R. Tedrake, I. R. Manchester, M. Tobenkin, and J. W. Roberts, "LQR-trees: Feedback motion planning via sums-of-squares verification," *The International Journal of Robotics Research*, vol. 29, no. 8, pp. 1038–1052, 2010.
- [23] S. M. LaValle, *Planning Algorithms*. Cambridge University Press, 2006.